JPE 19-2-13

https://doi.org/10.6113/JPE.2019.19.2.475
ISSN(Print): 1598-2092 / ISSN(Online): 2093-4718

Control and Modulation of Three to Asymmetrical Six-Phase Matrix Converters based on Space Vectors

Mohammed A. Al-Hitmi*, Khaliqur Rahman†, Atif Iqbal*, and Nasser Al-Emadi*

†,*Department of Electrical Engineering, Qatar University, Doha, Qatar

Abstract

This paper proposes the modulation and control of a three-to-six-phase matrix converter with an asymmetrical six-phase output. The matrix converter (MC) outputs consist of two sets of three-phase spatially shifted by 30^0, where the two sets have two isolated neutrals. The space vector approach is considered for the modeling and subsequent modulation of the three-to-six phase MC. The intelligent selection of voltage space vectors is made to synthesize the reference voltages and to obtain a sinusoidal output. The dwell times of selected voltage space vectors are adjusted in such a way that the effect of the second and the third auxiliary plane vectors (i.e., *x1-y1*, and *x2-y2*) are nullified. To achieve the maximum output voltage gain and to ensure that no reactive power is drawn from the utility supply, the input side power factor is maintained at unity. Nevertheless, the source side power factor is controllable. The modulation technique is implemented in dSPACE working in conjunction with a FPGA. Hardware results that validate the proposed control algorithm are discussed.

Key words: Asymmetrical, multiphase, Matrix converter, Modeling of converter, Space vector pulse width modulation

I. INTRODUCTION

Multiphase drives have been receiving increased attention from the industry and academia due to their essential advantages when compared to their three-phase equivalents. This is especially true in high-power and medium-voltage drive applications where reliability is a crucial concern. Multiphase motor drives offer various benefits such as torque pulsation at a higher frequency, reduced per phase current, reduced per-leg converter rating, higher fault tolerance, the possibility of independently controlling more than one motors when supplied by only one multi-leg converter [1]. These features make them attractive for many high-power medium-voltage industrial applications. Most of the literature on multiphase motor drive systems discusses six-phase systems because they are a multiple of the existing phase number of three [2]-[4]. This makes the control techniques a simple extension of the applicable methods of three-phase systems.

There are two basic types of six-phase motors configurations: symmetrical and asymmetrical. The symmetrical structures consist of six windings having a phase displacement of 60^0. In the asymmetrical structure, two sets of balanced three-phase windings are displaced by 30^0 in space [5]-[8].

It has been observed that there are a lot of harmonic currents if space vectors PWM (SVPWM) is extended from the concepts of a three-phase system. The dedicated control strategy to mitigate harmonics is complicated due to its complex converter-machine model. Transformation in the d-q-0 reference frame helps in developing simplified control algorithms for the machine [9], [10]. For a six-phase system, a space vector decomposition control technique is proposed in [6]. In this control technique, the six-dimensional space vector is divided into three two-dimensional orthogonal subspaces. Thus, it is now possible to model the machine with three sets of decoupled equations.

In a variable speed motor drive system, the electric machine is supplied through either an inverter or a MC. Most studies illustrate multiphase inverter-fed motor drive systems. However, a MC offers some other advantages not available in inverter-based drives. The MC is a bi-directional AC-AC converter without a bulky capacitor. The significant advantages offered by MCs are: i) bi-directional power flow, ii) capacitor free power exchange, iii) sinusoidal source current, and iv) controllable input power factor [11]-[13]. However, in MC control, a larger

Manuscript received May 9, 2018; accepted Jan. 2, 2019
Recommended for publication by Associate Editor Young-Doo Yoon.
†Corresponding Author: k.rahman@qu.edu.qa
Tel: +97477222641, Qatar University
*Dept. of Electrical Eng., Qatar University, Qatar

number of active components are required, and the complexity is significantly higher.

Generally speaking, there are two types of MC: direct and indirect. Numerous techniques have been reported in the literature for the control of a conventional MC with a three-phase input and a multi-phase output. A MC fed multiphase motor drive system was recently introduced in [14]-[18]. In these papers, five-phase induction motors were mainly discussed. Limited six phase research work was reported in [17], [18]. In these papers, the six-phase induction motor is fed by a six-phase inverter or a MC. A direct modulation algorithm was proposed in [18]. Direct control is simple for realization purposes. However, precision and flexibility in control are difficult to achieve.

In the recent past, both carrier-based and SVPWM schemes for multiphase MCs have been developed [19]-[21]. However, the emphasis was placed on the SVPWM methods [22]-[25]. The carrier-based PWM method is a lot simpler for execution. However, many of the properties of multiphase systems are not immediately observable. Consequently, the SVPWM control technique has been predominately under research. Hence, in this paper, the same technique is investigated and reported. Therefore, six phase MC control followed by space vector pulse width modulation is performed. This is used to control a double 3-phase isolated load as a first stage for showing the benefits of using this technology. This paper presents the implementation of a testing environment for one of the most promising multi-phase solutions.

This paper is structured as follows. Section II presents the modelling of a three-to-six phase indirect MC, where the possibilities of the switching states and their proper selection are explained. In section III, SVPWM control for a three-to-six phase MC is explained. In section IV, switching selection and their sequence of operation is presented. In section V, some simulation results are presented. In section VI, the algorithm is implemented in a field-programmable gate array (FPGA) and is tested using a six-phase asymmetrical *R-L* load. Section VII analyses the obtained results. Finally, section 8 draws some conclusions.

II. Modeling of a Three-To-Six Phase Matrix Converter

Based on conversion stages, a MC can be direct or indirect. In this paper, a direct MC based on an indirect approach is considered for modulation and control. The indirect MC has two conversion stages. These are the rectification and inversion stages. A power circuit diagram of a three-to-six phase indirect MC with a dual three-phase load is shown in Fig. 1. The MC consists of a rectifier and an inverter connected with a fictitious dc link. The input of the rectifier of the indirect MC is a three-phase balance AC source.

For MC control, the output voltage and the input current

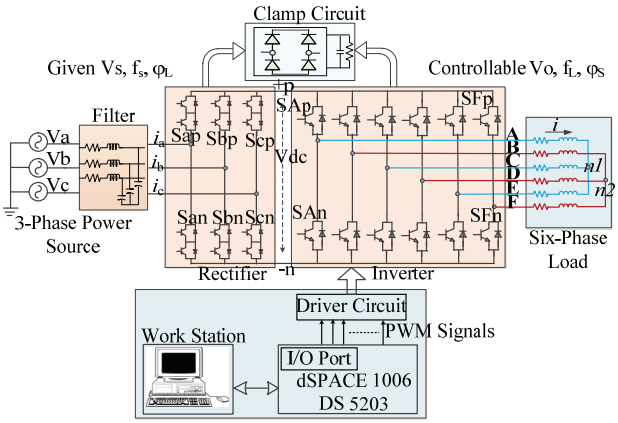

Fig. 1. Diagram of the proposed three-to-six phase MC.

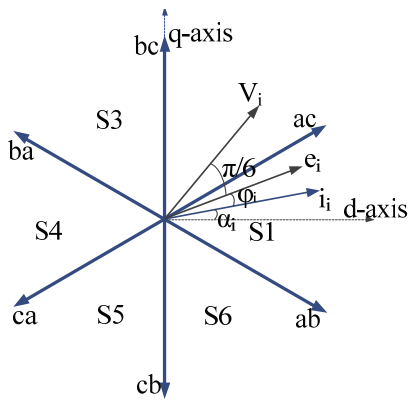

Fig. 2. Current space vectors of the rectifier stage of a MC.

displacement angle ϕ_i, are taken as reference quantities. Since the input phase voltage vector e_i is imposed by the source voltages and is also determined by measurements, the control of ϕ_i can be achieved by controlling the phase α_i of the input current vector [26]. Therefore, it is essential to control the input current and output voltage reference for the control of the MC. The parameters ϕ_i, α_i and e_i are shown in Fig. 2.

A. Modeling of the Three-Phase Rectifier

It is assumed that the source is balanced in Fig. 1, where S_i ($i = a, b, c$) is the switching function. When S_i =1 ($i = a, b, c$), the above bridge arm is ON, while the lower bridge arm is OFF. Therefore, the switching function S_i is defined as:

S_i=1: the upper bridge arm is "ON" and the lower bridge arm is "OFF".

S_i=0: the upper bridge arm is "OFF" and the lower bridge arm is "ON"

A space vector diagram of the input currents, obtained from equation (1), is shown in Fig. 2.

$$\bar{i}_i = \frac{2}{3}\left(i_a + \kappa i_b + \kappa^2 i_c\right), \kappa = e^{j\frac{2\pi}{3}} \tag{1}$$

There are nine possible switching combinations that lead to the generation of nine different current space vectors. These

TABLE I
OUTPUT VOLTAGE SPACE VECTORS IN THE D-Q PLANE (K IS SECTOR NUMBER THAT VARIES FROM THE 1ST TO 12TH SECTOR)

Number of vectors	Vector representation	Space vectors
4	0,63,21,38	$0.0\ V_{ab,bc,ca}$
12	41,54,25,36,26,45,22,9,39,27,37,18	$0.1728\ V_{ab,bc,ca}\times e^{j(2k-1)\frac{\pi}{12}}$
24	32,53,16,58,40,61,20,62,8,29,4,46, 10,31,5,47,2,23,1,43,34,55,17,59	$0.3333\ V_{ab,bc,ca}\times e^{j2k\frac{\pi}{12}}$
12	50,57,52,24,44,30,13,6,11,39,19,33	$0.4714\ V_{ab,bc,ca}\times e^{j(2k-1)\frac{\pi}{12}}$
12	49,48,56,60,28,12,14,15,7,3,35,51	$0.6439\ V_{ab,bc,ca}\times e^{j(2k-1)\frac{\pi}{12}}$

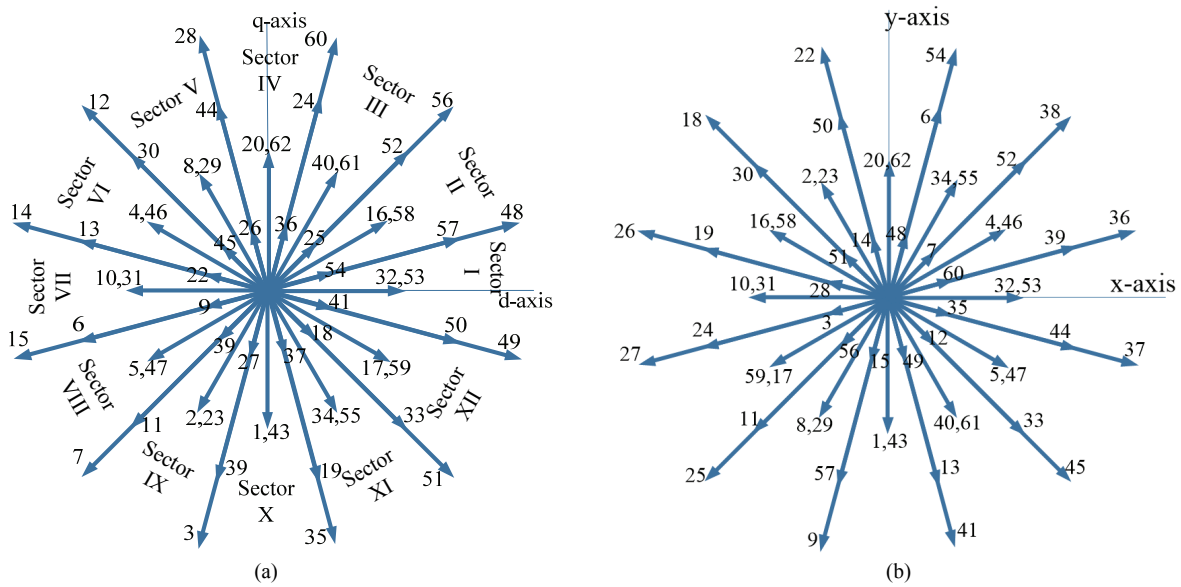

Fig. 3. Active voltage space vectors for an inverter in a three-to-six phase MC. (a) In the *d-q* plane. (b) Component in the *x-y* plane.

space vectors are spanned over six sectors (*S1, S2…,* and *S6*). *S1* indicates the first sector that spans from -30^0 to 30^0. The three-phase sinusoidal input voltage is divided every 60°, where a PWM cycle is divided into six intervals. Thus, only one phase current changes its direction in one PWM cycle in any of the sectors. The switch modes include the I_1 *(ac)*, I_2 *(bc)*, I_3 *(ba)*, I_4 *(ca)*, I_5 *(cb)* and I_6 *(ab)* vectors. Moreover, three zero vectors can be obtained by simultaneously turning 'ON' the upper and lower switches of the same leg of the rectifier, while keeping other phases 'OFF'.

B. *Modeling of an Asymmetrical Six-phase VSI*

In the inverter stage, all of the possible $2^6 = 64$ vectors are placed in 24 different directions in space forming four regular polygons. These voltage vectors divide the plane into 12 sectors, each panning 30^0. The output voltage vectors in the space *d-q*, *x-y* and 0^+-0^- orthogonal planes can be defined by equations (2)-(4). The positions of these vectors with their amplitudes in a different sector are presented in Table I.

Among them, only the large and second large length polygons vectors and two zero vectors have been selected for the implementation of SVPWM. Thus, 26 space vectors are employed for synthesizing the reference, and the other 38 space vectors are discarded.

The space vectors $V_{d\text{-}q}$ and $V_{x\text{-}y}$ are shown in Fig. 3(a) and Fig. 3(b), respectively. These vectors form four concentric

$$\overline{V_{d-q}} = \frac{2}{6}(e^{j0}v_{AB} + e^{j\frac{\pi}{6}}v_{BC} + e^{j\frac{2\pi}{3}}v_{CD} + e^{j\frac{5\pi}{6}}v_{DE} + e^{j\frac{4\pi}{3}}v_{EF} + e^{j\frac{9\pi}{6}}v_{FA}) \quad (2)$$

$$\overline{V_{x-y}} = \frac{2}{6}(e^{j0}v_{AB} + e^{j\frac{5\pi}{6}}v_{BC} + e^{j\frac{8\pi}{6}}v_{CD} + e^{j\frac{\pi}{6}}v_{DE} + e^{j\frac{4\pi}{6}}v_{EF} + e^{j\frac{9\pi}{6}}v_{FA}) \quad (3)$$

$$\overline{V_{0^+-0^-y}} = \frac{2}{6}(e^{j0}v_{AB} + e^{j\frac{6\pi}{6}}v_{BC} + e^{j\frac{12\pi}{6}}v_{CD} + e^{j\frac{18\pi}{6}}v_{DE} + e^{j\frac{24\pi}{6}}v_{EF} + e^{j\frac{30\pi}{6}}v_{FA}) \quad (4)$$

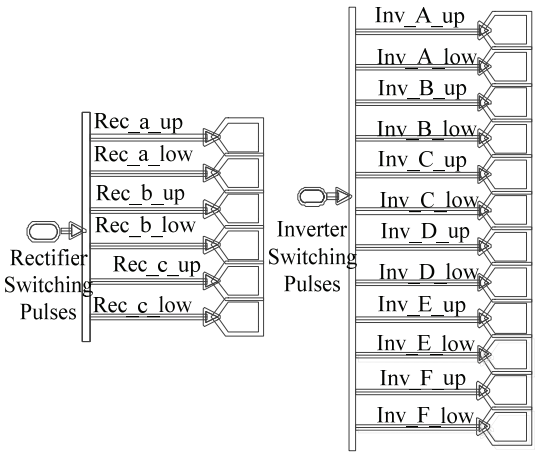

(a)

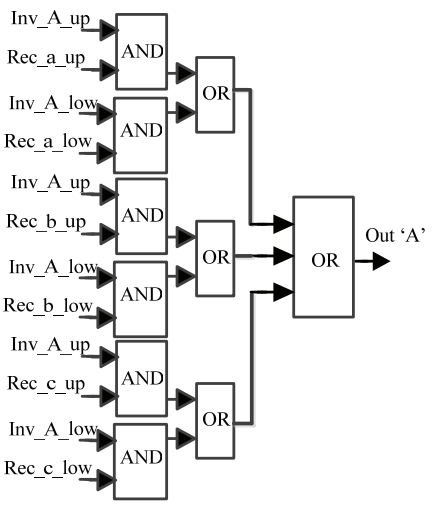

(b)

Fig. 4. Mapping of rectifier and inverter switching pulses. (a) Switching pulses of the rectifier and inverter. (b) Mapping to form the output phase 'A'.

polygons. The lengths of the output voltage vectors are:

$$V_l = 0.6439 \ \ p.u, V_{Sl} = 0.4714 \ \ p.u, V_m = 0.3333 \ \ p.u, V_S = 0.1725 \ \ p.u.$$

Here, the per unit is based on the output line voltage.

Six switching pulses for the rectifier switches and twelve switching pulses for the inverter switches are developed in the modulation. However, in the laboratory, these rectifier and inverter switching pulses are mapped to directly control the MC eighteen switches. The mapping is further explained with the help of Fig. 4.

III. Space Vector PWM of a Three-to-Six Phase Matrix Converter

A. Space Vector PWM Control of Input Current

The input reference current is determined by two neighboring current vectors. Thus, the input reference current in sector S1 can be decomposed along the two adjacent space vectors i_γ and

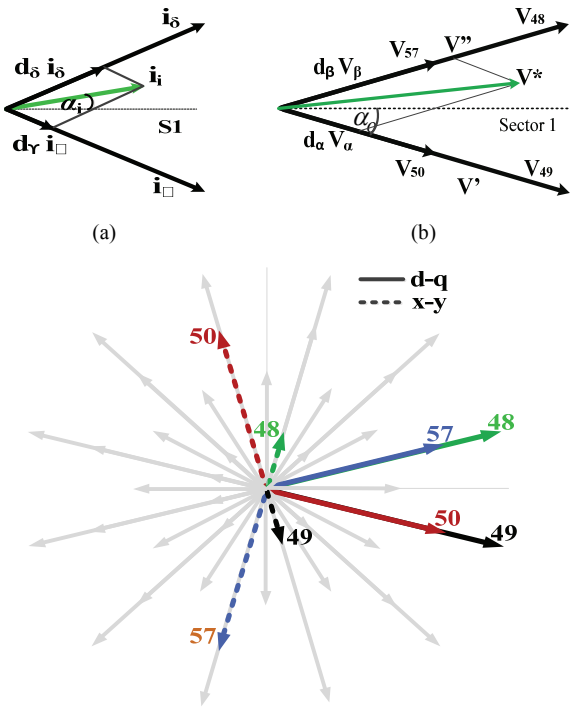

Fig. 5. Active voltage space vectors in three-to-six phase matrix converter. (a) Input current space vectors for S1. (b) Reference vector control. (c) Active voltage space vectors for sector-I in d-q and their component in x-y plane.

i_δ shown in Fig. 5(a). The duty cycles of the current vectors of the rectifier stage can be expressed as:

$$d_\gamma = \frac{T_\gamma}{T_s} = m_r \times \sin\left(\frac{\pi}{3} - \alpha_i\right) \quad (5)$$

$$d_\delta = \frac{T_\delta}{T_s} = m_r \times \sin(\alpha_i) \quad (6)$$

$$d_0 = \frac{T_0}{T_s} = 1 - d_\gamma - d_\delta \quad (7)$$

Where T_s is the time to complete one switching cycle, and m_r is the modulation index (MI) of the rectifier stage. This is defined as:

$$0 \le m_r = I_i / I_{dc} \le 1 \quad (8)$$

B. Space Vector PWM Control of Output Voltage

There are eight voltage space vectors in sector-I. Among them, {41, 54} are small vectors, {50, 57} are second large vectors (V_{Sl}), {48, 49} are large vectors ((V_l) and the remaining two {32, 53} lie inside the sector (can be named as non-vertex vectors). For obtaining a sinusoidal waveform with low total harmonic distortion (THD), V_{ref} is generated by four adjacent V_l and V_{Sl} non-zero vectors and two zero vectors. The dwell time of the switching vectors of sector-I for the selected vectors are calculated and presented in equations (9)-(13).

TABLE II
SWITCHING CONFIGURATION FOR A MC WITH ITS CORRESPONDING OUTPUT VOLTAGES AND CURRENTS

Sec. 1	A	B	C	D	E	F	V_{AB}	V_{BC}	V_{CD}	V_{DE}	V_{EF}	V_{FA}	i_a	i_b	i_c
I_0(bb)-V_{42}	b	b	b	b	b	b	0	0	0	0	0	0	0	0	0
I_6(ab)-V_{50}	a	a	b	b	a	b	0	V_{ab}	0	$-V_{ab}$	V_{ab}	$-V_{ab}$	$+i_a$	$-i_a$	0
I_6(ab)-V_{48}	a	a	b	b	b	b	0	V_{ab}	0	0	0	$-V_{ab}$	$+i_a$	$-i_a$	0
I_6(ab)-V_{49}	a	a	b	b	b	a	0	V_{ab}	0	0	$-V_{ab}$	0	$+i_a$	$-i_a$	0
I_6(ab)-V_{57}	a	a	a	b	b	a	0	0	V_{ab}	0	$-V_{ab}$	0	$+i_a$	$-i_a$	0
I_0(aa)-V_{21}	a	a	a	a	a	a	0	0	0	0	0	0	0	0	0
I_1(ac)-V_{57}	a	a	a	c	c	a	0	$-V_{ca}$	0	V_{ca}	$-V_{ca}$	V_{ca}	$-i_c$	0	$+i_c$
I_1(ac)-V_{49}	a	a	c	c	c	a	0	$-V_{ca}$	0	0	0	V_{ca}	$-i_c$	0	$+i_c$
I_1(ac)-V_{48}	a	a	c	c	c	c	0	$-V_{ca}$	0	0	V_{ca}	0	$-i_c$	0	$+i_c$
I_1(ac)-V_{57}	a	a	c	c	a	c	0	0	$-V_{ca}$	0	V_{ca}	0	$-i_c$	0	$+i_c$
I_0 (cc)-V_{42}	c	c	c	c	c	c	0	0	0	0	0	0	0	0	0

$$d_\alpha = \frac{T_\alpha}{T_s} = m_v.\sin(30^0 - \alpha_o) \quad (9)$$

$$d_\beta = \frac{T_\beta}{Ts} = m_v.\sin(\alpha_o) \quad (10)$$

$$d_{0I} = \frac{T_{0I}}{Ts} = 1 - d_\alpha - d_\beta \quad (11)$$

$$0 \le m_v = x.V_o / V_{dc} \le 1 \quad (12)$$

For sector I,

$$0 \le \alpha_o = (\omega_o t + 30^0) \le +30^0 \quad (13)$$

Here, d_α, d_β and d_{0I} are the duty ratios for the voltage space vectors in the directions shown in Fig. 5(b). These times of operation can be adjusted among the vectors lying in their direction. m_v is the MI of the inverter that is the ratio of the peak output voltage and the fictitious DC link voltage. The reference voltage vector angle is α_o.

The proposed control technique aims to reduce the THD to get a sinusoidal output current. To achieve this, the effect of the *x-y* component in the output should be eliminated or minimized [23]. To achieve the minimum *x-y* effect, the selection of space vectors and their operation times are essential. For sector-I of the inverter, the position of the voltage vectors and their *x-y* components are shown. The large vector with -15^0 angles has a small length x-y component in the direction of 75^0. Similarly, this is shown for all four active vectors. Just by a proper adjustment of the voltage×time application of the vectors, the effect of the *x-y* component can be eliminated, i.e. a large vector causing a smaller x-y operated for longer than the second large vector. The operation time is shared as $V_{48}\times t_{48}=V_{57}\times t_{57}$.

On the other hand, if six active vectors in a sector are applied for reference control, the *x-y* mapping is not exactly in phase opposition, which restricts the cancellation of *x-y*. For this reason, the effect of *x-y* is present in the output, which causes more losses. Thus, only large and second large voltage vectors are selected. In the proposed control, nullifying the effect of the *x-y* plane space vectors is elaborated in Fig. 5(c). The cancelation of the *x-y* plane vectors is illustrated for sector-I, and the same concept is applied to the other eleven sectors.

IV. SWITCHING CONTROL OF A MATRIX CONVERTER USING SVPWM

The active switching states for the resulting output voltage in sector-I of the inverter and the input current of the rectifier are tabulated in Table II. In the third row, the switch configuration of the rectifier allows the flow of the current i_a through input phase 'a' and $-i_a$ through input phase 'b'. This means the input phases 'a' and 'b' conduct to get output voltage at the inverter output terminals. In the inverter stage, the input phase 'a' is connected to the output phase legs 'A', 'B' and 'E' and the input phase 'b' is connected with the output phase legs 'C', 'D' and 'F'. In a switching cycle, the total number of commutations is 16.

There are eight active switching combinations for sector-I. These combinations are shown in Table II with their respective output voltages and input currents. The overall output voltage formation for a complete switching cycle of a three-to-six phase MC for sector I is shown in Fig. 6. The reference current vector I_{ref} is synthesized from the two vectors I_{ab} and I_{ac}. Where I_{aa} is used as a zero current vector. The output reference voltage vector located in sector-I in the inverting stage follows the sequence V_{42}-V_{50}-V_{48}-V_{49}-V_{57}-V_{21}-V_{57}-V_{49}-V_{48}-V_{50}-V_{42}.

Fig. 7 shows the locus of the maximum output of the voltage space vector in the linear operating range that is displayed by V_{s_max}.

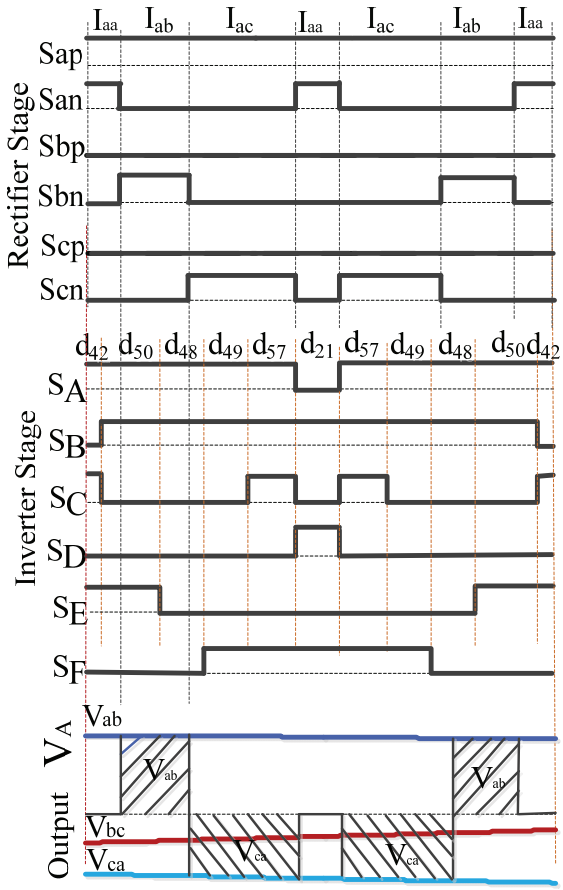

Fig. 6. Synthesis of the output voltage of a matrix converter.

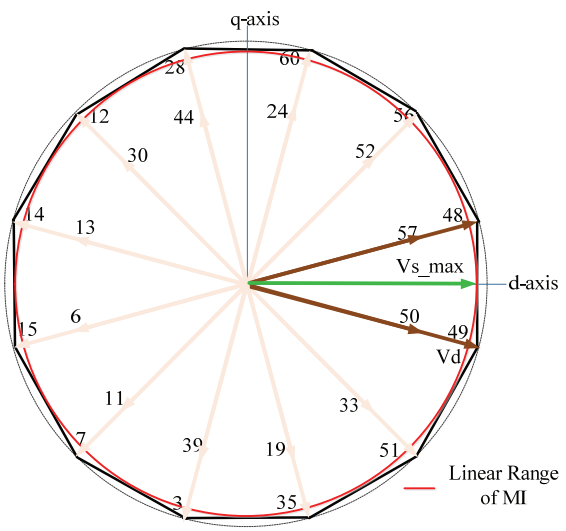

Fig. 7. Locus of the achievable range of a reference voltage vector for SVPWM in the linear operating range.

V. Simulation Results

Due to the presence of discontinuous input currents, the MC behaves as a source of current harmonics, which are injected back into the AC mains. Since these current harmonics result in voltage distortions that affect the overall operation of the AC system, they have to be reduced. Therefore, it becomes necessary to use an input filter, which is the interface between the voltage fed source and the converter [27]. Meeting the requirements an L-C filter is achieved in the lab with the parameters 0.0032 H and 6 μF. With an inductance, a resistance of 0.9 ohm is connected in series.

TABLE III
Simulation Parameters

Source voltage	V_{phase}= 100 V
Load parameters (R-L load)	R = 40 Ω, L = 140 mH
Switching frequency	f_{sw} = 2 kHz
Input frequency (f_{in})	f_{in}=50 Hz
Output frequency	f_o=25 Hz, 60 Hz

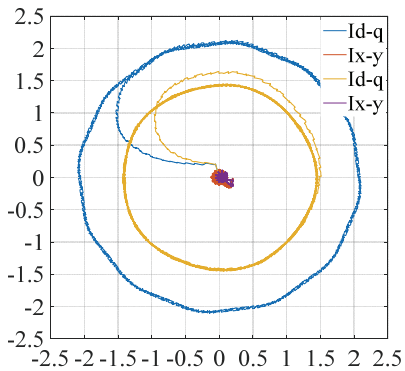

Fig. 8. d-q and x-y components in the load current.

A simple *R-L* load is considered to validate the control scheme of a three-to-six phase MC fed asymmetrical six phase load system. The simulation parameters are shown in Table III. The simulation is presented at two different output frequencies of 25 Hz and 60 Hz. These frequencies are chosen to illustrate the viability of the control technique for a large range of operating frequencies. Moreover, it works in the full linear range of MI of the MC. The simulation is performed at a MI of 0.8 p.u.

The effectiveness of the schemes is observed by the nature of the waveforms and the voltage transferred to the load. Two sets of three-phase voltages are obtained at the output of the MC, which can be used to feed an asymmetrical six-phase load. The d-q and x-y components in the load currents are shown in Fig. 8 at two different frequencies. The x-y component is almost eliminated. The line voltages across the load are shown with their spectrums in Fig. 9(a) and 9(b). Fig 9(c) and 9(d) show the unity power factor operation of the MC since the grid voltage and filtered input current are in the same phase. The voltage harmonic spectrum shows that the switching frequency component of the harmonics and their sidebands are present and that double the switching frequency is the dominant frequency. This results in a lower contribution in the THD since the switching frequency is much greater than the modulation frequency.

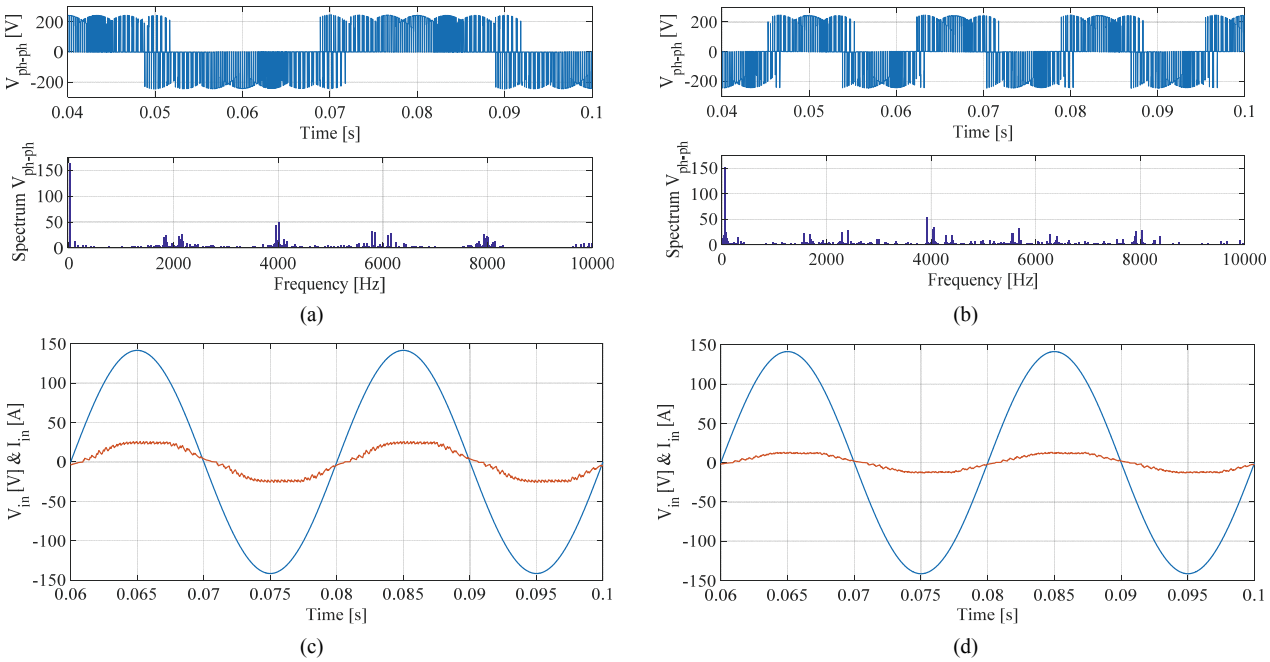

Fig. 9. Simulation results for a three-to-six MC at MI = 0.8. (a) Output Vph-ph with spectrum, at f_o = 25 Hz. (b) Output Vph-ph with spectrum, at f_o = 60 Hz. (c) Source voltage and current at f_o = 25 Hz. (d) Source voltage and current at f_o = 60 Hz.

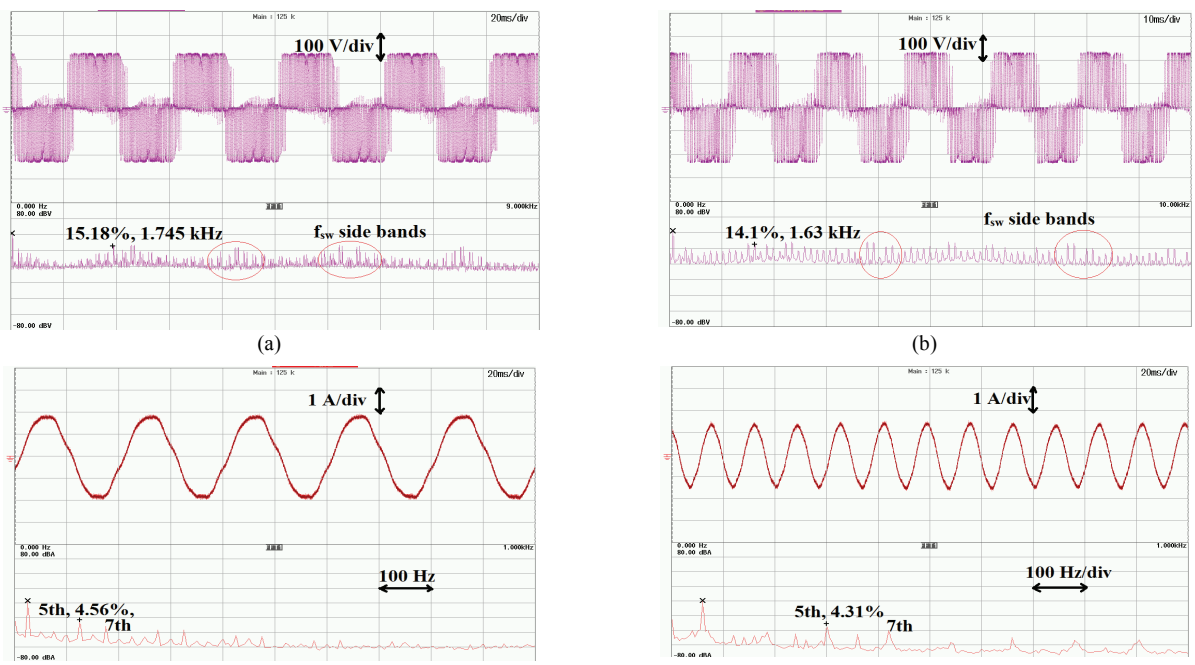

Fig. 10. Experimental results for a three-to-six phase MC at MI=0.8. (a) Output Vph-ph with spectrum, at f_o=25 Hz, [X-axis: 20ms/div, Y-axis: 100V/div]. (b) Output Vph-ph with spectrum, at f_o=60 Hz, [X-axis: 10ms/div, Y-axis: 100V/div]. (c) Load current at f_o=25 Hz [X-axis: 20ms/div, Y-axis: 1 A/div]. (d) Load current at f_o=60 Hz [X-axis: 20ms/div, Y-axis: 1 A/div].

VI. Experimental Results

For the testing and validation of the analytical and simulation results, a prototype of a three-to-six phase MC is developed in the laboratory. The control code for the MC control is generated in a system generator and build in dSPACE 1006 in combination with a FPGA board DS 5203. In the turn ON and turn OFF processes of two switches of the same leg, a dead band of 2 μs is given. For the creation of the dead band, an external Xilinx FPGA controller is used, which is programmed in VHDL. The experimental and simulation parameters are the same. Experimental results are presented in Fig. 10 and Fig. 11.

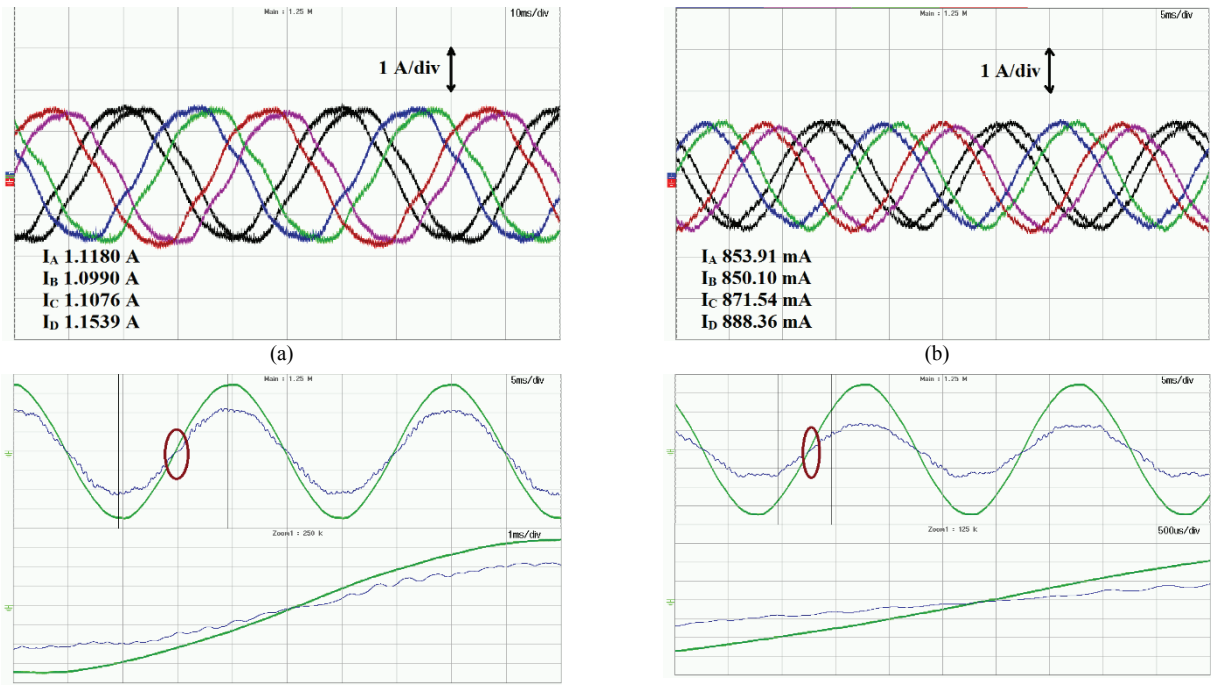

Fig. 11. Experimental results of a three-to-six phase MC. (a) Balanced load currents at f_o = 25 Hz. (b) Balanced load currents at f_o = 60 Hz. (c) Source voltage and current at f_o = 25 Hz. (d) Source voltage and current at f_o = 60 Hz.

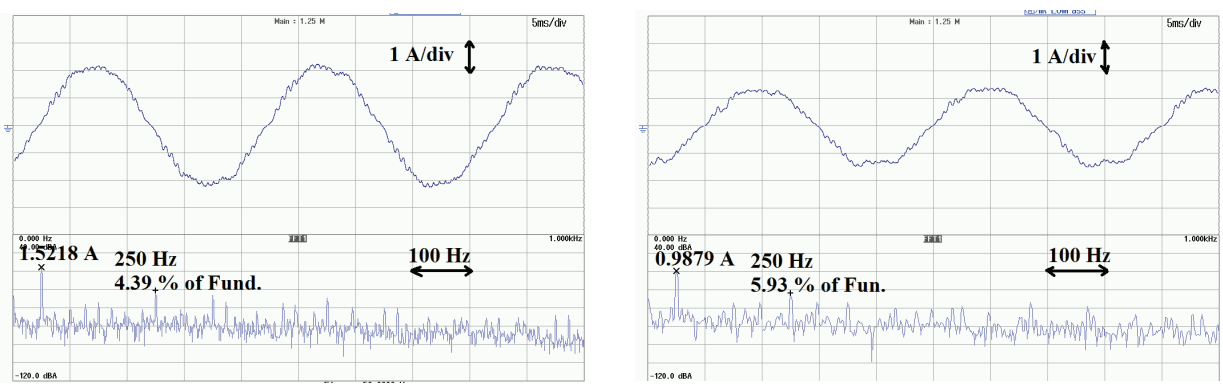

Fig. 12. Experimental results of a three-to-six phase MC. (a) i_a with spectrum at the output frequency f_o = 25 Hz. (b) i_a with spectrum at the output frequency f_o = 60 Hz.

To test the proposed MC based load system, a wide range of operating frequencies and modulation indices have been taken. Fig. 10(a) and 10(b) show output voltage waveforms along with FFT spectra for an R-L load at operating frequencies of 25 Hz and 60 Hz at a MC MI of 0.8 p.u. It can be observed that there are large harmonic components that appear as sidebands in the neighbourhood of multiples of the switching frequency. Fig. 10(c) and 10(d) show the load current with its THD spectrum. Fig. 11(a) and 11(b) confirm the balanced operation of the three-to-six phase MC. Meanwhile, operation at a unity power factor at the input side is confirmed from Fig. 11(c) and Fig. 11(d). It is observed that input voltage and current maintain a unity power factor and that the output current is almost sinusoidal.

Filtered source current is shown in Fig. 12(a) and 12(b) for 25 and 60 Hz, respectively. This shows that lower order harmonics are present. The first dominating harmonic is the fifth order which is 4.39 % of the fundamental at 25 Hz and 5.93% at 60 Hz of output frequency operation. There are large harmonics in the source current that may be due to dead time operation and improper filter value selection.

VII. Performance Analysis and Discussion

With the help of simulation and experimental results, the proposed control technique is validated. In this section, the performance factors are considered. These factors include the output voltage, THD, switching losses and efficiency. Based

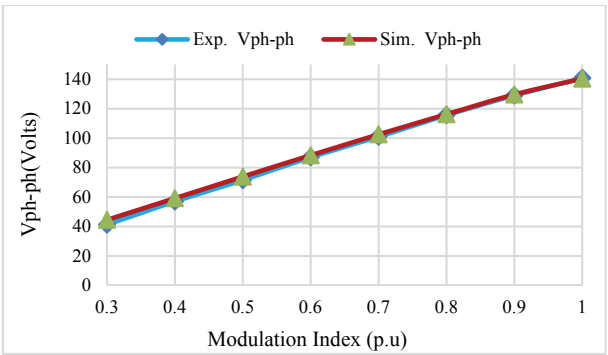

(a)

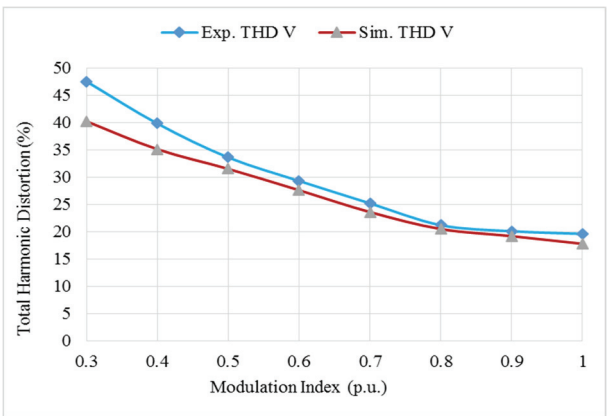

(b)

Fig. 13. Three-to-six phase matrix converter. (a) Voltage transferred to the load. (b) THD in the output line voltage.

on these factors, the proposed system is analyzed from the obtained results.

A. Voltage Transferred to the Load

In the linear range of operation, the six-phase inverter has a maximum output in [28], $1/[2\cos(\Pi/12)] = 0.5176*V_{dc}$. Meanwhile, the length of the largest rectifier equivalent of the input side can be written as $0.66V_{dc}$. Here, V_{dc} is the magnitude of the output voltage of the fictitious dc link. Thus, the total maximum output of the MC can be written as a ratio of the largest six-phase inverter output and the largest space vector length of the input side rectifier. This comes to 0.7764. Meanwhile, the transfer limit decreases with an increase in phase number. That is 0.7886 and 0.7693 in a three-to-five MC and a three-to-seven phase MC, respectively.

Hence at the output of the MC, only 0.7764 times the input voltage can be obtained with the proposed control method of SVPWM. The total output of the MC at different MI is plotted and shown in Fig. 13(a). It is found that the output voltage of the MC varies almost linearly with the MI. Experimental and simulation results are well matched for the full linear range of operation.

B. Total Harmonic Distortion in the Output Voltage

Since the MC produces switched output voltage of the fundamental frequency, the distortion in the output voltage is mainly due to the switching frequency and its sidebands. The THD in the output voltage is graphed and presented in Fig. 13(b) for simulation and experimental results. The experimentally obtained output voltage has a higher THD than the simulated one. This difference is mainly due to the non-ideal conditions in the experiment in in comparison with the ideal conditions used in the simulation. The main reasons for this include the effects of sampling time and dead time. The sampling time of the experimental code is 20 µs. Meanwhile, it is only 2 µs in the simulation. The larger sampling time results in higher harmonics. Moreover, a 2 micro-second dead time between the 'on' and 'off' of the two switches is provided. Meanwhile, dead time operation is not considered in the simulation. This results in a significant variation in the simulated and experimentally obtained THD values. In the SVPWM, the control variables follow the desired references in a sector. When the reference signal has to be increased, the time for the application of large vectors is also increased, which is accompanied by a decrease in the time of the application of the second large vectors. It is observed that with an increase in the MI, the THD in the output voltage decreases in the linear range of operation of the MC.

C. Switching and Power Loss Analysis

There are switching and conduction losses in the switches of the matrix converter. The conduction loss is proportional to the forward voltage drop across the switch and the current carried by the IGBT. The conduction loss is the sum of the conduction loss in the IGBT and its associated diode. This is formulated in (14).

Therefore, the conduction loss in the MC is slightly higher than that of the inverter. There are switching losses during the switch state transitions. The switching losses are also proportional to the switching frequency of the converter [29], [30].

D. Matrix Converter Losses

The conduction losses of the converter can be written as equation (14). This is a product of a voltage drop during forward conduction, the average current in the switch and the duty cycle of the switch.

$$P_{con,ph} = \sum_{n=1}^{3} \left[\left(V_{cen} I_{cn} d_n \right) + \left(V_{fn} I_{fcn} d_n \right) \right] \tag{14}$$

Where V_{ce} is saturation voltage, I_c is the IGBT collector current, V_f is the diode forward voltage drop, and I_f is the diode current in the forward condition. In addition, the switching loss in a switch of the MC can be calculated as a product of the energy loss in a pulse and the switching frequency. It is given as:

$$P_{sw,ph} = 3 f_s \times E_{loss} \tag{15}$$

The total loss of the converter is the sum of the conduction and the switching loss.

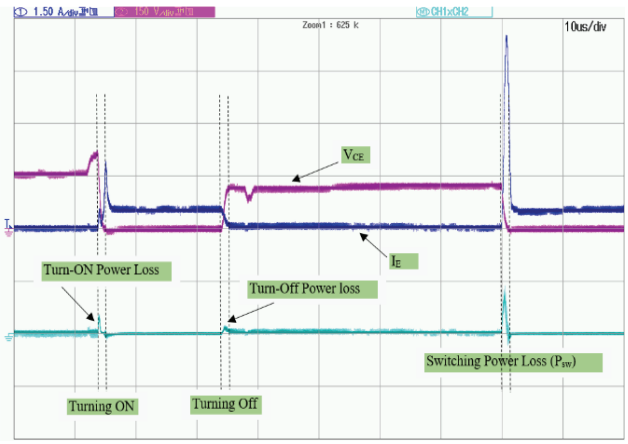

(a)

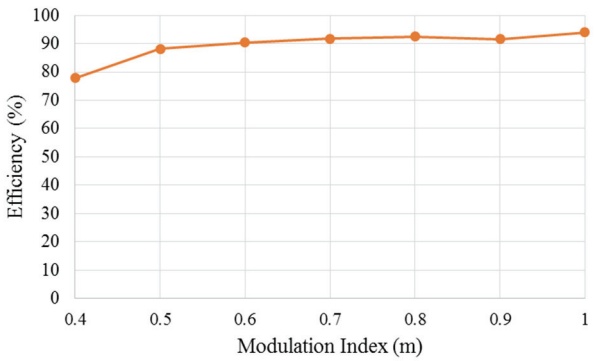

(b)

Fig. 14. Three-to-six phase matrix converter. (a) Power loss during a switching state transition and conduction. (b) Converter efficiency.

$$P_{loss} = 6\left(P_{con,ph} + P_{sw,ph}\right) \tag{16}$$

The switching power loss in an IGBT of a three-to-six phase MC is shown in Fig. 14(a). A SKM75GB128D, a reference voltage 600 Volt and 50 Amp IGBTs are used. The other electrical parameters are E_{ON}= 6 mJ per pulse, E_{Off} = 8 mJ per pulse, V_{CEO}=1.15 V, V_F = 0.8 V and r_{CE} = 24 mΩ.

The power loss of the three-to-six phase MC is calculated for the linear range of the modulation index. The output frequency is 50 Hz, and load parameters are the same as the experimental load. Measurements include the input and output power to the MC. The remaining power is the power loss during switching and the clamp circuit loss due to dead time operation during phase transitions.

$$\eta_{conv} = \frac{P_{out}}{P_{in}}, \quad \mathrm{P_{in}} = \sum_{in=a,b,c} V_{in} I_{in} \cos(\phi_i) \tag{17}$$

$$\mathrm{P_{out}} = \sum_{out=A...E} V_{out} I_{out} \cos(\phi_o) \tag{18}$$

Where, V_{in}, I_{in} and ϕ_I are the input voltage, current and input power factor angle, respectively. The operation is maintained at a unity power factor. V_{out}, I_{out} and ϕ_0 are the output voltage, current and output power factor angle, respectively. Fig. 14(b) shows the experimentally tested efficiency of the proposed three-to-six phase MC at different MI. There are two major contributors for the losses in the converter. The losses due to the switches and losses due to the clamping circuit. The efficiency of the converter is higher when operated at higher modulation indices. The clamp circuit consumes a significant amount of energy. Therefore, a method should be devised to reduce such losses.

VIII. Conclusions

In this paper, a SVPWM for a three-to-six phase MC fed to a six-phase asymmetrical load with an isolated neutral has been developed and analyzed. The detailed modeling and the SVPWM are presented. An intelligent switching sequence and the dwell time for the selected switches in a switching cycle have been given. Since the load is asymmetrical, the phase displacement between the voltage vectors of the inverting stage is maintained at 30^0 between two sets of isolated three-phase loads. The space vectors in the *d-q* plane are controlled to nullify the effect of the *x-y* plane vectors. The other aim is set to achieve sinusoidal operation of the MC up to the maximum attainable output voltage. A three-to-six phase MC is implemented experimentally, and the SVPWM control is verified by waveforms of the voltages and the corresponding harmonic spectra. The operation is verified for a wide range of operating frequencies and the full linear range of the modulation index. Furthermore, a loss calculation is done and presented for the calculation of the efficiency of the MC. Simulation and experimental results are presented, which validate the effectiveness of the proposed control algorithm.

Acknowledgment

This publication was made possible by Qatar University internal grant QUCP-CENG-17/18-2. The statements made herein are solely the responsibility of the authors.

References

[1] E. Levi, "Advances in converter control and innovative exploitation of additional degrees of freedom for multiphase machines," *IEEE Trans. Ind. Electron.*, Vol. 7, No. 4, pp. 433-448, Jan. 2016.

[2] I. Gonzalez-Prieto, M. J. Duran, J. J. Aciego, C. Martin, and F. Barrero, "Model predictive control of six-phase induction motor drives using virtual voltage vectors," *IEEE Trans. Ind. Electron.*, Vol. 65, No. 1, pp. 27-37. Jan. 2018.

[3] D. Glose and R. Kennel, "Continuous space vector modulation for symmetrical six-phase drives," *IEEE Trans. Power Electron.,* Vol. 31, No. 5, pp. 3837-3848, May 2016.

[4] D. Glose and R. Kennel, "Carrier-based pulse width modulation for symmetrical six-phase drives," *IEEE Trans. Pow. Electron.,* Vol. 30, No. 12, pp. 6873-6882, Dec. 2015

[5] M. A. Abbas, R. Christen, and T. M. Jahns, "Six-phase voltage source inverter driven induction motor," *IEEE Trans. Ind. Appl.*, Vol. IA-20, No. 5, pp. 1251-1259, Sep. 1984.

[6] Y. Zhao and T. A. Lipo, "Space vector PWM control of dual three-phase induction machine using vector space decomposition," *IEEE Trans. Ind. Appl.*, Vol. 31, No. 5, pp. 1100-1109, Sep./Oct. 1995.

[7] C. Wang, K. Wang, and X. You, "Research on synchronized SVPWM strategies under low switching frequency for six-phase VSI-fed asymmetrical dual stator induction machine," *IEEE Trans. Ind. Electron.,* Vol. 63, No. 11, pp. 6767-6776, Nov. 2016.

[8] K. Marouani, L. Baghli, D. Hadiouche, A. Kheloui, and A. Rezzoug, "A new PWM strategy based on a 24-sector vector space decomposition for a six-phase VSI-fed dual stator induction motor," *IEEE Trans. Ind. Electron.*, Vol. 55, No. 5, pp. 1910-1920, May 2008.

[9] R. Bojoi, E. Levi, F. Farina, A. Tenconi, and F. Profumo, "Dual three-phase induction motor drive with digital current control in the stationary reference frame," *IEE Proceedings - Electric Power Applications*, Vol. 153, No. 1, pp. 129-139, Jan. 2006.

[10] E. Levi, M. Jones, S. N. Vukosavic, and H. A. Toliyat, "Steady-state modeling of series-connected five-phase and six-phase two-motor drives," *IEEE Trans. Ind. Appl.*, Vol. 44, No. 5, pp. 1559-1568, Sep./Oct. 2008.

[11] A. Alesina and M. Venturini, "Analysis and design of optimum amplitude nine-switch direct ac-ac converters," *IEEE Trans. Power Electron.,* Vol. 4, No. 1, pp. 101-112, Jan. 1989.

[12] A. K. Koiwa and J.I.Itoh, "A maximum power density design method for nine switches matrix converter using SiC MOSFET," *IEEE Trans. Power Electron.*, Vol. 31, No. 2, pp. 1189-1202, Feb. 2016.

[13] A. Alesina and M. Venturini, "Solid state power conversion: A fourier analysis approach to generalised transformer synthesis," *IEEE Trans. Circuit Syst.,* Vol. 28, No. 4, pp. 319-330, Apr. 1981.

[14] Y. Guo and X. Yan, "Research on matrix converter control multi-phase PMSM for all electric ship," *International Conference on Electrical and Control Engineering*, pp. 3120-3123, 2011.

[15] S. M. Dabour, A. Abdel-Khalik, S. Ahmed, and A. Massoud, "Performance of a three-to-five matrix converter fed five-phase induction motor under open-circuit switch faults," *IEEE Symposium on Computer Applications & Industrial Electronics (ISCAIE)*, pp. 159-164, 2016.

[16] A. Iqbal, R. Alammari, H. Abu-Rub, and S. M. Ahmed, "PWM scheme for dual matrix converters based five-phase open-end winding drive," *IEEE International Conference on Industrial Technology (ICIT)*, pp. 1686-1690, 2013.

[17] E. A. R. Engku Ariff, O. Dordevic, and M. Jones, "A space vector PWM technique for a three-level symmetrical six-phase drive," *IEEE Trans. Ind. Electron.*, Vol. 64, No. 11, pp. 8396-8405, Nov. 2017.

[18] H. Wang, R. Zhao, F. Cheng, and H. Yang, "Six-phase induction machine driven by the matrix converter," *International Conference on Electrical Machines and Systems*, pp. 1-5, 2011.

[19] A. Iqbal, S. M. Ahmed, and H. Abu-Rub, "Space vector PWM technique for a three to five-phase matrix converter," *IEEE Tran. Ind. Appl.* Vol. 48, No. 2, pp. 697-707, Mar. 2012.

[20] K. Rahman, A. Iqbal, and R. Al-ammari, "Space vector model of a three-phase to five-phase AC/AC converter," *Proc. IEEE AFRICON*, Mauritius, pp. 1-6, 2013.

[21] K. Rahman, A. Iqbal, A. A. Abduallah, R. Al-ammari, and H. Abu-Rub, "Space vector PWM technique for a three to seven phase direct matrix converter," *IEEE APEC,* pp. 595-601, 2014.

[22] P. Tenti, L. Malesani, and L. Rossetto, "Optimum control of N-input K-output matrix converters," *IEEE Trans. Power Electron.,* Vol. 7, No. 4, pp. 707-713, Oct. 1992.

[23] S. M. Ahmed, A. Iqbal, H. Abu-Rub, J. Rodriguez, C. A. Rojas, and M. Saleh, "Simple carrier-based PWM technique for a three-to-nine-phase direct AC-AC converter," *IEEE Trans. Ind. Electron.,* Vol. 58, No. 11, pp. 5014-5023. Nov. 2011.

[24] A. Iqbal, K. Rahman, R. Alammari, and H. Abu-Rub, "Space vector PWM for a three-phase to six-phase direct AC/AC converter," *IEEE International Conference on Industrial Technology (ICIT)*, pp. 1179-1184, 2015.

[25] M. Chai, D. Xiao, R. Dutta, and J. E. Fletcher, "Space vector PWM techniques for three-to-five-phase indirect matrix converter in the over modulation region," *IEEE Trans. Ind. Electron.* Vol. 63, No. 1, pp. 550-561, Jan. 2016.

[26] K. Rahman, A. Iqbal, N. Al-Emadi, and L. Ben-Brahim, "Common mode voltage reduction in a three-to-five phase matrix converter fed induction motor drive," *IET Power Electron.,* Vol. 10, No. 7, pp. 817-825, 2017.

[27] P. Wheeler and D. Grant, "Optimised input filter design and low-loss switching techniques for a practical matrix converter," *IEE Proceedings –Elect. Pow. Appl.*, Vol. 144, No. 1, pp. 53-60, Jan. 1997.

[28] N. B. de Freitas, C. B. Jacobina, A. C. N. Maia, and V. F. M. B. Melo, "Six-leg single-phase multilevel rectifier inverter: PWM strategies and control," *IEEE Tran. Ind. Appl.*, Vol. 53, No. 1, pp. 350-361, Jan./Feb. 2017.

[29] M. Trzynadlowski, R.L. Kirlin, and S.F. Legowski, "Space vector PWM technique with minimum switching losses and a variable pulse rate [for VSI]," *IEEE Trans. Ind. Electr.*, Vol. 44, No. 2, pp. 173-181, Apr. 1997.

[30] K. Zhou, L. Huang, X. Luo, Z. Li, J. Li, G. Dai, and B. Zhang, "Characterization and performance evaluation of the super junction RB-IGBT in matrix converter," *IEEE Trans. Power Electron.*, Vol. 33, No. 4, pp. 3289-3301, Apr. 2018.

Mohammed A. Al-Hitmi was born in Qatar, in 1968. He received his B.Sc. degree in Electrical Engineering from Qatar University, Doha, Qatar, in 1992; and his M.Sc. and Ph.D. degrees in Control Engineering from the University of Sheffield, Sheffield, ENG, UK, in 1994 and 2002, respectively. He is presently working as an Assistant Professor in the Department of Electrical Engineering, Qatar University. His current research interests include control systems theory, neural networks, fuzzy control and electric drive systems.

Khaliqur Rahman was born in Uttar Pradesh, India, in 1986. He received his B.Tech. and M.Tech. degrees from Aligarh Muslim University (AMU), Aligarh, India, in 2008 and 2010, respectively. From July 2010 to June 2012, he was a Lecturer in the Department of Electrical Engineering, Aligarh Muslim University. He received his Ph.D. degree from the Qatar University, Doha, Qatar in 2019. He is presently working as a Research Assistant in Qatar University. His current research interests include the modeling, simulation and control of multiphase power electronic converters.

Atif Iqbal received his B.Sc. (Gold Medal) and M.Sc. degrees in Power System and Drives Engineering from Aligarh Muslim University (AMU), Aligarh, India, in 1991 and 1996, respectively. He received his Ph.D. degree from the Liverpool John Moores University, Liverpool, ENG, UK, in 2006. He has been employed as a Lecturer in the Department of Electrical Engineering, AMU, since 1991, where he served as a Full Professor until August 2016. He is presently working as an Associate Professor in the Department of Electrical Engineering, Qatar University, Doha, Qatar. He was a recipient of an Outstanding Faculty Merit Award AY 2014-2015 and a Research Excellence Award at Qatar University. He received best research paper awards at IEEE ICIT-2013, IET-SEISCON-2013 and SIGMA 2018. His research findings related to power electronics and renewable energy sources have been published in a number of international journals and conference proceedings. Dr. Iqbal has authored/co-authored more than 300 research papers. He has also published one book and three chapters in two other books. He has supervised several large R&D projects. His current research interests include the modeling and simulation of power electronic converters, the control of multi-phase motor drives and renewable energy sources. He was a Fellow of IET (UK), a Fellow of IE (India) and a Senior Member of IEEE, PhD (UK). He served as an Associate Editor of the IEEE Transactions on Industry Application, and as Editor-in-Chief of i-manager's Journal of Electrical Engineering.

Nasser Al-Emadi received his B.Sc. and M.Sc. degrees in Electrical Engineering from Western Michigan University, Kalamazoo, MI, USA, in 1989 and 1994, respectively. He received his Ph.D. degree from Michigan State University, East Lansing, MI, USA, in 2000. He is presently serving as the Head and as an Associate Professor in the Department of Electrical Engineering, Qatar University, Doha, Qatar. His current research interests include electric power systems, the control, protection and sensor interfacing of multi-phase motor drives and renewable energy sources, as well as the integration of smart grids. He has been published in a number of international journals and conference proceedings. He also holds a number of international patents. Dr. Al-Emadi has co-authored a book and two chapters in two other books. He has supervised several large R&D projects. He was a founding member of Qatar Society of Engineers, a Member of IEEE and an Advisory Board Member of the IEEE Qatar Section.